PAPER

Large-area synthesis and photoelectric properties of few-layer MoSe$_2$ on molybdenum foils

View the article online for updates and enhancements.

IOP ebooks™

Bringing you innovative digital publishing with leading voices to create your essential collection of books in STEM research.

Start exploring the collection - download the first chapter of every title for free.

Large-area synthesis and photoelectric properties of few-layer MoSe$_2$ on molybdenum foils

Zenghui Wu[1,2]**, Guoan Tai**[1,2] ⬤**, Xufeng Wang**[1,2]**, Tingsong Hu**[1,2]**, Rui Wang**[1,2] **and Wanlin Guo**[1]

[1] The State Key Laboratory of Mechanics and Control of Mechanical Structures, Laboratory of Intelligent Nano Materials and Devices of Ministry of Education, College of Aerospace Engineering, Nanjing University of Aeronautics and Astronautics Nanjing 210016, People's Republic of China
[2] School of Material Science and Technology, Nanjing University of Aeronautics and Astronautics Nanjing 210016, People's Republic of China

E-mail: taiguoan@nuaa.edu.cn

CrossMark

Abstract

Compared with MoS$_2$ and WS$_2$, selenide analogs have narrower band gaps and higher electron mobilities, which make them more applicable to real electrical devices. In addition, few-layer metal selenides have higher electrical conductivity, carrier mobility and light absorption than the corresponding monolayers. However, the large-scale and high-quality growth of few-layer metal selenides remains a significant challenge. Here, we develop a facile method to grow large-area and highly crystalline few-layer MoSe$_2$ by directly selenizing the Mo foil surface at 550 °C within 60 min under ambient pressure. The atomic layers were controllably grown with thicknesses between 3.4 and 6 nm, which just met the thickness range required for high-performance electrical devices. Furthermore, we fabricated a vertical p–n junction photodetector composed of few-layer MoSe$_2$ and p-type silicon, achieving photoresponsivity higher by two orders of magnitude than that of the reported monolayer counterpart. This technique provides a feasible approach towards preparing other 2D transition metal dichalcogendes for device applications.

Supplementary material for this article is available online

Keywords: few-layer MoSe$_2$, chemical vapor deposition, photoelectric properties, transition metal dichalcogendes, photodetectors

(Some figures may appear in colour only in the online journal)

1. Introduction

Two-dimensional (2D) transition metal dichalcogenides (TMDs, e.g., MoS$_2$, WS$_2$, MoSe$_2$, WSe$_2$, MoTe$_2$ and WTe$_2$) with a significant band gap have recently attracted much interest owing to their unique electronic, optical, magnetic and thermal properties for various applications in light-emitting devices, photo-detectors, solar cells and field effect transistors [1–9]. Monolayer TMDs have a 'three-layer' structure consisting of nonmetallic (S, Se or Te) at the top and bottom layers sandwiching Mo layers [3, 10]. In few-layer counterparts within 2–10 layers, the layers are stacked together with weak van der Waals interactions between the nonmetallic atoms [3, 5, 11]. With the thickness decrease in semiconducting TMDs, such as molybdenum- and tungsten-based dichalcogenides, their band gaps are transformed from indirect for a bulk or multilayer counterpart to direct for a monolayer due to quantum confinement effects [5, 12, 13]. However, the inherent monolayer thickness possesses a vast challenge in the weak interaction between light and the mono-layers, which results in poor light emission and absorption behavior [7, 14, 15]. In comparison with the monolayers, the density of states of few-layer TMDs is three times that of the

corresponding monolayer [16], and exceptional physical phenomena, such as strong electroluminescence, high carrier mobility, saturable absorbing and remarkable light absorption, have been observed in the few layers [7, 16–18]. The exceptional physical properties give rise to a large range of applications in high-performance field effect transistors, high-speed flexible electronics and phototransistors [7, 16–23]. In particular, TMDs within 2–7 nm in thickness are very suitable for fabricating high-performance electrical devices [7].

Among the 2D TMDs, molybdenum selenide ($MoSe_2$) is considered as an important semiconductor, superior to the corresponding sulfides in optoelectronics and electronics applications owing to the inherent advantages of a smaller band gap of 1.55 eV in monolayer $MoSe_2$ than that of 1.9 eV in monolayer MoS_2, a ten-fold narrower line width and tunable excitonic charging effects compared with monolayer MoS_2. Few-layer $MoSe_2$ possesses tailorable attributes and designed functionalities due to layer-number-dependent optical and electrical properties, and the band gap varies from 1.55 eV in a monolayer to 1.1 eV in a bulk counterpart, which will be beneficial to high-efficiency photoelectronic and photovoltaic devices [24, 25]. In experimental realization, a mechanically exfoliated technique using Scotch tape from the bulk was found to be unsuitable for constructing large-scale integrated devices due to the obtained small size [24]. The chemical vapor deposition (CVD) method is a potential technique for few-layer $MoSe_2$ thin films towards large-area applications in optoelectronic devices [5, 26–28]. Fashionable CVD techniques have concentrated on the selenation of Mo films or molybdenum compounds (such as MoO_3 and $MoCl_5$) to prepare few-layer $MoSe_2$ thin films on diverse substrates such as SiO_2/Si and sapphire; however, they are unable to synthesize large-area, uniform, easy transferable and highly crystalline $MoSe_2$ atomic layers [5, 26–29]. Molecular beam epitaxy had been developed to grow large-scale few-layer $MoSe_2$ with high quality, but it was not beneficial to industrial applications due to its high cost [5, 30]. Therefore, the controllable preparation of large-scale, uniform, easily transferable and highly crystalline few-layer $MoSe_2$ is of urgently importance to meet the high requirement of fabricating advanced photoelectronic and photovoltaic devices on an industrial scale. Here, we report a facile method to grow uniform and highly crystalline few-layer $MoSe_2$ over the order of centimeters by directly selenizing annealed Mo foil surfaces in selenium (Se) vapor at 550 °C for 60 min under atmospheric pressure. After preparation, the obtained films are easily transferrable to various substrates by removing the Mo foil using a diluted ferric chloride ($FeCl_3$) solution. The thickness of the thin films transferred onto a 285 nm SiO_2/Si substrate is in the range of 3.4 to 6 nm, which perfectly falls in the range of 2–7 nm for the best performance of electronic devices. To demonstrate the potential in photoelectric device applications, we fabricated a vertical p–n junction photodetector composed of few-layer $MoSe_2$ and p-type silicon.

2. Experimental details

2.1. Growth and transfer of few-layer $MoSe_2$

Typically, a molybdenum foil (20 μm, 99.95%), 5 cm in length and 1 cm in width, was degreased and cleaned by acetone, IPA and ethanol, respectively. Then, it was annealed at 1400 °C for 10 h under an atmosphere of 50 sccm H_2, which induced recrystallization to enlarge the crystal grain boundaries on the Mo foils (figures S1(a), (b) are available online at stacks.iop.org/NANO/29/125605/mmedia). The detailed CVD procedure for preparing the few-layer $MoSe_2$ is as follows: firstly, a Mo foil was put into a quartz tube located at the growth zone; secondly, 500 mg selenium powders (99.999% purity, Alfa Aesar) inside a quartz crucible were put on the source zone, which was located upstream from the Mo foils, and the zone was heated to a temperature of 250 °C with a high-temperature ceramic heating ring for 10 min under 10 sccm Ar gas; thirdly, the growth zone was heated to 550 °C at a rate of 20 °C min^{-1} and carrier gas flow of 10 sccm, and it was kept at this temperature for different durations from 1 to 120 min (figure S2); fourthly, the source zone was cooled to room temperature with the assistance of an electric fan for 3 min; finally, the furnace was opened and cooled to room temperature naturally for over 30 min. As such, few-layer $MoSe_2$ was prepared by the CVD procedure at atmospheric pressure using ultrahigh-purity argon as the carrier gas. After the growth, $MoSe_2$ atomic layers at one-side of the Mo foil were removed by mechanical grinding. PMMA was initially spin-coated onto the other side of the as-synthesized sample. The Mo foils were dissolved using 2 M iron chloride. Afterwards, the $MoSe_2$ coated PMMA was transferred onto a 285 nm SiO_2/Si substrate and the PMMA layer was removed in hot acetone. The few-layer $MoSe_2$ could also be easily transferred onto different substrates such as PDMS, PET, SiO_2/Si, quartz and glass.

2.2. Structural characterization of $MoSe_2$ film

Optical microscopy of Olympus BX41 was employed to capture the morphology of the few-layer $MoSe_2$. Atomic force microscopy (AFM, SmartSPM, HORIBA Scientific) was used to obtain the thickness profile of the as-synthesized $MoSe_2$ films. Field emission scanning electron microscopy (FESEM) images were captured on a ZEISS Merlin. Transmission electron microscopy (TEM) images and selected area electron diffraction (SAED) patterns were performed using a JEM 2100F FESEM (JEOL, Tokyo, Japan) working at 200 kV. Raman spectra were recorded using an Evolution Raman microscope from HORIBA scientific with an excitation laser of 532 nm and an estimated laser spot size of 2 μm. Chemical state and elemental composition analyses were performed using x-ray photoelectron spectroscopy (ESCALAB 250, Thermo Fisher Scientific Inc) with focused monochromatized AlKa irradiation.

2.3. Fabrication and measurement of few-layer MoSe₂–Si heterojunction devices

To fabricate the few-layer MoSe$_2$/p-Si heterojunction photodetectors, we selected p-type Si wafers with a resistivity of 0.1–0.5 Ω cm, which corresponded to a boron doping level of 3×10^{16}–10^{17} cm^{-3}. The detailed preparation process of the MoSe$_2$/p-Si devices was as follows: (1) a wafer 4 in in diameter was first cut into smaller pieces of 1×1 cm^2 in size; (2) the natural oxide layer on the Si substrate was removed by immersing it into 5% diluted hydrofluoric acid (HF) for 2 min; (3) a 0.2×0.2 cm^2 photosensitive area for the photodetectors was determined by a blue tape (Nitto Tape); (4) 300 nm SiO$_2$ was deposited on the p-Si wafers by a sputtering process; (5) a 0.3×0.3 cm^2 window of the photodetectors, which contained the photosensitive area, was also defined by a blue tape; (6) a gold thin film with 150 nm thickness was deposited on the 300 nm SiO$_2$ on Si substrates to fabricate a square electrode. The process was performed using magnetron sputtering equipment (Quorum Q150T). The equipment was evacuated down to 10^{-3} Pa and then the pressure was raised to, and kept at, 1 Pa under argon gas. After that, the sputtering process was started and the deposition rate was 13 nm min^{-1}. (7) Few-layer MoSe$_2$ was transferred onto the surface of the square electrode and photosensitive area on the Si substrates. Note: (a) the adhesive residues from the blue tape were removed by acetone over 30 min; (b) before transferring MoSe$_2$ thin films, a final dip in 5% HF solution for 3 s was carried out to remove any native oxide that may have regrown during the fabrication process; (8) the MoSe$_2$-Si photodetector was heated at 150 °C for 30 min in vacuum to enhance the electrical contact. In the photodetectors, the Au thin films contacted with the MoSe$_2$ films acted as a negative electrode, and silver conductive paint dots contacted with the bottom of the p-Si acted as a positive electrode. The electrical properties of the photodetectors were measured by a Keithley 2400 sourcemeter in darkness and light conditions. A commercial red LED with a 625 nm wavelength was used as the illuminated light. All the measurements were performed at room temperature.

3. Results and discussion

3.1. Synthesis and characterization of few-layer MoSe₂

In our work, a high-temperature tube furnace was used for the CVD synthesis of few-layer MoSe$_2$. A schematic diagram of the growth setup is displayed in figure 1(a). The atomic structure of the MoSe$_2$ atomic layers is indicated in the a, b and c directions, as shown in figure 1(b). Typically, the annealed foil surface was selenized by selenium vapor and the MoSe$_2$ was controllably grown on the Mo foils at 550 °C for 60 min (figures 1(c), S1(c) and (d)). Furthermore, the thin film was successfully transferred onto various substrates for further characterization and device application (figure 1(d)).

The morphology of the obtained few-layer MoSe$_2$ samples was characterized by scanning electron microscopy

(SEM). It was observed that an atomically smooth MoSe$_2$ film was produced on the Mo foil surface, and the thin film had large grain boundaries of more than 50 μm in size, which was in good agreement with those for the pure annealed Mo foil (figure 1(c) and S1(b)). Optical microscopy was used to characterize the micro-scale morphology of the obtained MoSe$_2$ thin film, and the optical contrast between the thin films and the SiO$_2$/Si substrate showed that the film was continuous and nearly uniform in a large area (figure 1(d)).

Raman spectroscopy and AFM were utilized to further investigate the crystal quality and thickness of few-layer MoSe$_2$ on 300 nm SiO$_2$/Si substrates, as shown in figure 2. The Raman spectrum shows that the two intense peaks are E_{2g} and A_{1g} modes of MoSe$_2$ films, which grew at 550 °C for 1, 10, 30, 60 and 120 min, respectively (figure 2(a)). The prominent A_{1g} Raman mode and the weak E_{2g} Raman mode can be assigned to out-of-plane vibration of Se atoms and in-plane vibration of two Se atoms with respect to the Mo atom, respectively. Figures 2(b)–(f) show AFM images of the thin films grown at 550 °C for 1, 10, 30, 60 and 120 min, respectively. The AFM images show that the thickness of the MoSe$_2$ film grown at 550 °C for 1 min is around 3.4 nm; the value is 4.1 nm when prolonging the reaction time up to 10 min, then it becomes 6.0 nm when further increasing the reaction time to 60 min and finally it slightly decreases to 5.0 nm for longer reaction time up to 120 min, which indicates that the films consisted of 5–9 layers. Additionally, the location of Raman modes can be used to determine the thickness of 2D materials [29, 31, 32]. Being consistent with the reported values [33, 34], in our work, the A_{1g} mode of 5 L MoSe$_2$ is located at 233.3 cm^{-1}; along with the increase of the reaction time, the mode is blue-shifted to 235.1 cm^{-1} for 6 layers and finally to 236.9 cm^{-1} for 7- and 9-layer MoSe$_2$. Nevertheless, the E_{2g} modes stay at 285.6 cm^{-1} due to the relative thickness. The frequency difference between the E_{2g} and A_{1g} modes is another important indicator of determining the thickness of 2D materials, but different substrates or synthesis methods may cause deviations from the ideal values. We found that the frequency difference decreases with the increase of the layer numbers, and the values are 52.7, 50.5 and 46.9 cm^{-1} for 5, 6 and 7 or 9 layers, respectively. The stiffening of the A_{1g} mode may result from the increase in the van der Waals interaction between the layers, while the softening of the E_{2g} mode may be caused by the presence of long-range coulomb interactions between the layers [29, 35]. Similar phenomena have been previously observed in other 2D materials including GaSe, h-BN, MoS$_2$ and graphene [36–38].

The crystal structure and quality of the few-layer MoSe$_2$ prepared by the direct selenization process were further characterized by TEM. It was found that the ultrathin MoSe$_2$ atomic layers cover the holes of the TEM grid, as shown in figure 3(a). The high-magnification TEM image shows that the MoSe$_2$ atomic layer is uniform and continuous, as shown in figure 3(b). The high-resolution TEM image in figure 3(c) and the corresponding SAED pattern in the inset show that the film exhibits a polycrystalline characteristic. Furthermore, a high-resolution TEM (HRTEM) image reveals that the film
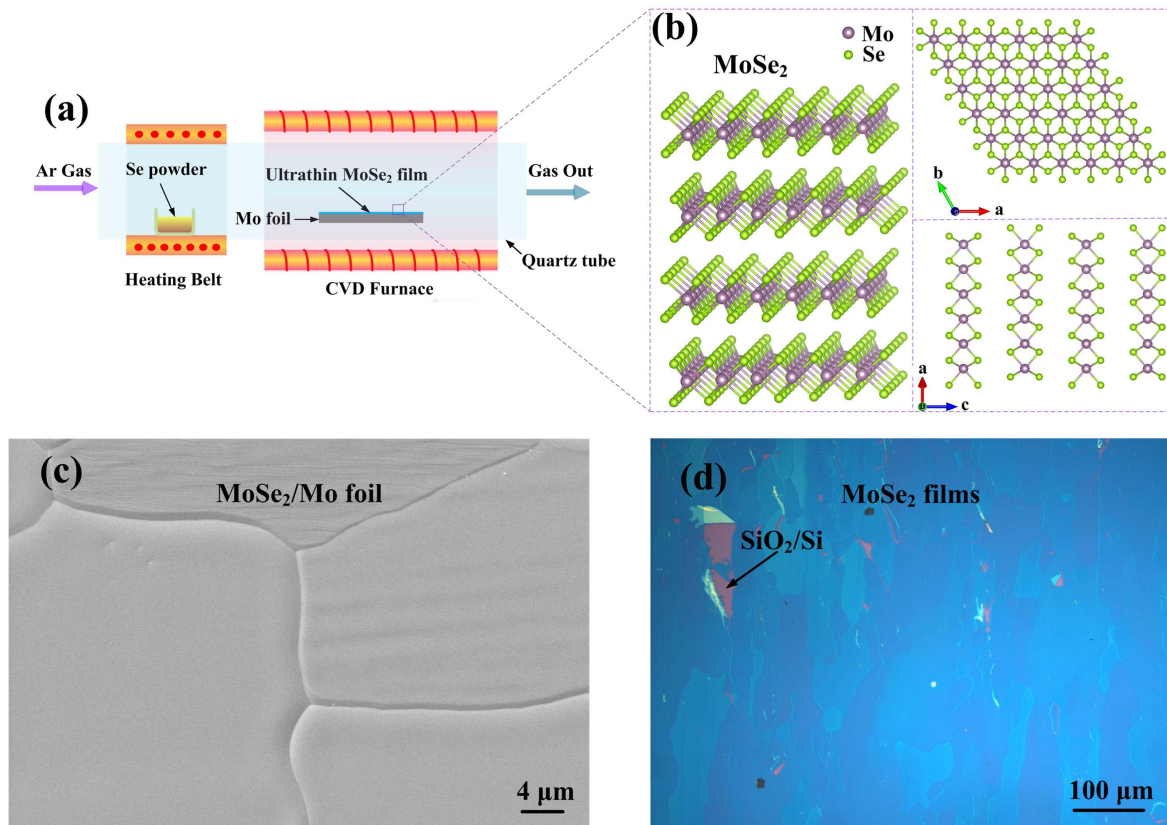
Figure 1. (a) Schematic illustration of the growth setup for synthesizing few-layer $MoSe_2$ grown by selenizing the annealed Mo foil surface at 550 °C for 60 min. (b) Atomic structure of $MoSe_2$ atomic layers shown in the *a*, *b* and *c* directions. (c) SEM image of the $MoSe_2$ atomic layers on the Mo foil. (d) Optical image of the $MoSe_2$ atomic layers on the Mo foil transferred onto a 285 nm SiO_2/Si substrate.
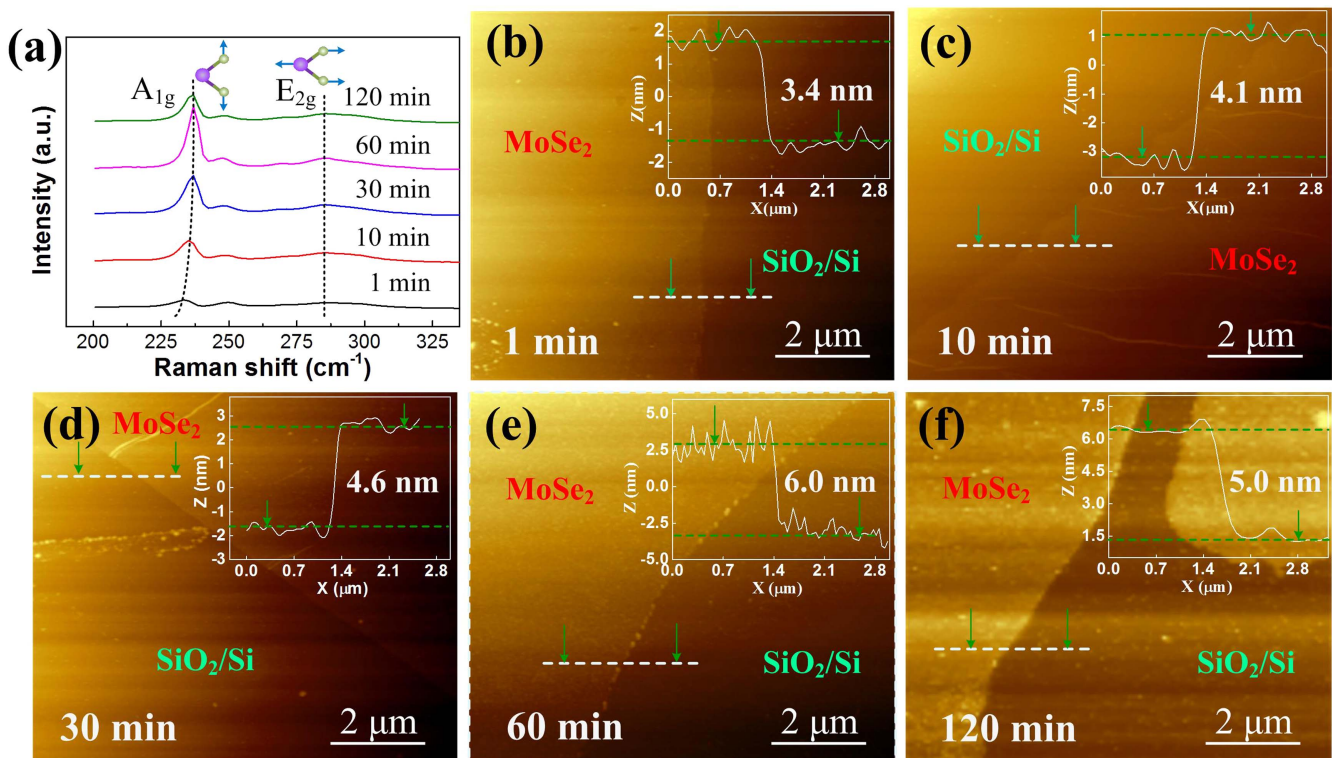
Figure 2. Raman spectra of few-layer $MoSe_2$: (a) Raman spectra of $MoSe_2$ atomic layers grown at various durations. (b)–(f) AFM images of $MoSe_2$ atomic layers grown at various durations. The thickness is varied from 3.4 to 6.0 nm. All the AFM images were performed on 300 nm SiO_2/Si substrates.
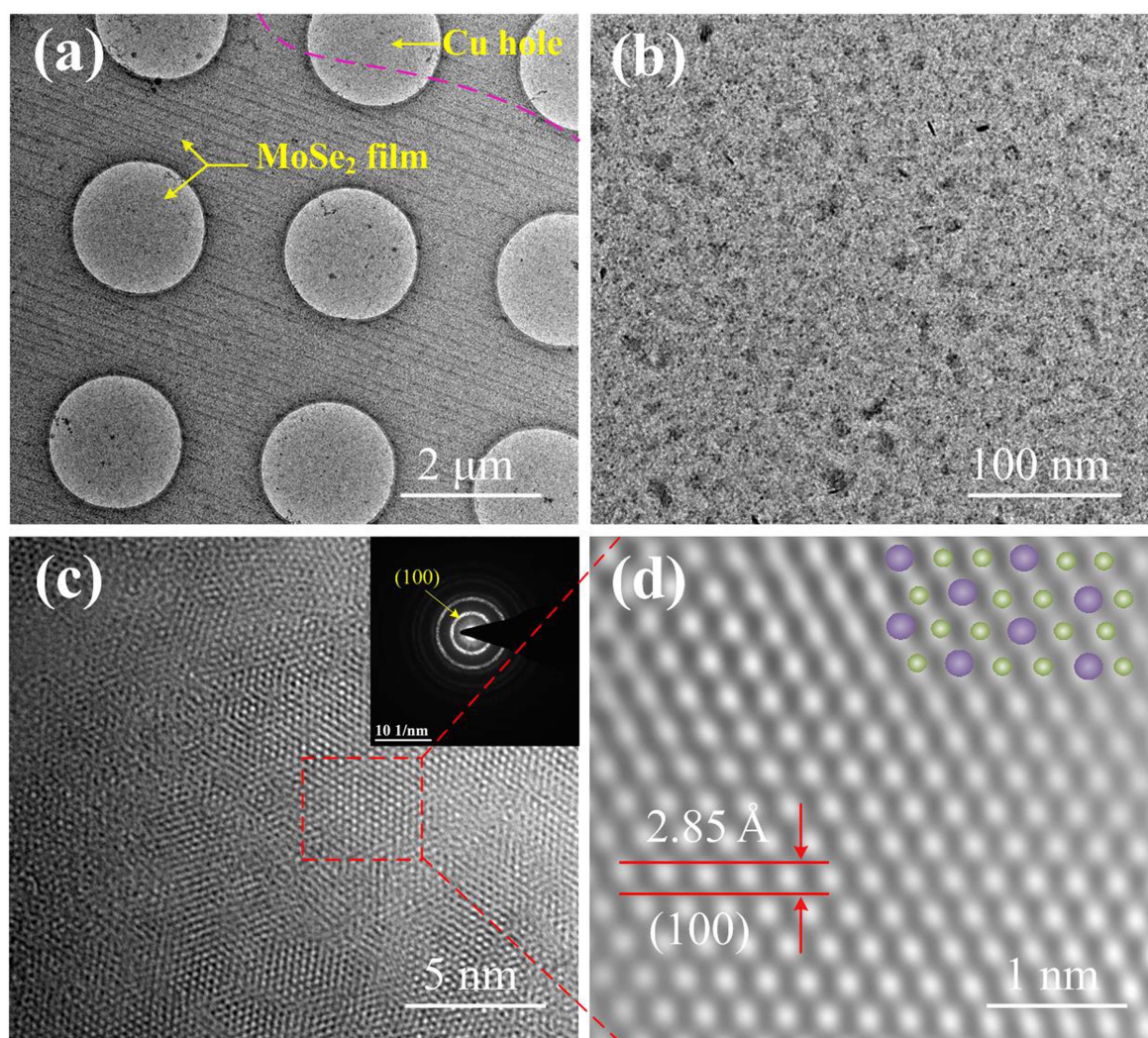
Figure 3. (a) Low-magnification TEM image of MoSe$_2$ atomic layers covering a TEM grid. (b) TEM image of the MoSe$_2$ atomic layers over a hole of the TEM grid. (c) HRTEM image of the MoSe$_2$ atomic layers. The inset is the corresponding SAED pattern. (d) Reconstructed HRTEM image by masking the FFT pattern, indicating clearly that the structure of the thin film has a character of 2H MoSe$_2$ atomic layers. The lattice spacings of 2.85 Å can be indexed into the (100) crystal faces of 2H MoSe$_2$. The inset shows the hexagonal arrangement of Mo and Se atoms.

has a 2H hexagonal lattice structure. To clearly index the lattice orientations, the corresponding MoSe$_2$ atomic layer was reconstructed by masking the fast Fourier transform (FFT) pattern (figure 3(d)) and the result indicated the 2H hexagonal lattice structure of MoSe$_2$ with a lattice spacing of 2.85 Å, which corresponded to (100) planes. The right top of figure 3(d) shows the hexagonal lattice model with Mo and Se atoms. The lattice constant of the 2D hexagonal lattice is measured directly from the image and determined to be $a = 3.329$ Å, which is in good agreement with that of the bulk MoSe$_2$ with a space group of P63/mmc [34, 39–41]. In addition, the TEM images of the MoSe$_2$ thin films grown at 550 °C with various durations were characterized to investigate the growth process and reveal the nucleation mechanism (figure S3).

X-ray photoelectron spectroscopy (XPS) was adopted to provide information not only about the chemical stoichiometry but also about the bonding of Mo and Se atoms in the

few-layer MoSe$_2$ on 300 nm SiO$_2$/Si substrate (figures 4(a)–(b)). The high-resolution XPS spectra show that the binding energies of Mo 3d$_{3/2}$ and Mo 3d$_{5/2}$ in the Mo 3d spectrum are respectively located at 231.7 and 228.6 eV, which could be attributed to the Mo^{4+} chemical states in MoSe$_2$ (figure 4(a)) [31]. In addition, a peak at 229 eV can be attributed to Se 3 s. The weak peaks located at 229.4 and 232.5 eV can be indexed to Mo^{4+} 3d$_{5/2}$ and 3d$_{3/2}$ of MoO$_2$, respectively. The other two weak peaks at around 232.5 and 235.7 eV can be respectively indexed to Mo^{6+} 3d$_{5/2}$ and 3d$_{3/2}$ of MoO$_3$. The 3d$_{5/2}$ of the MoO$_3$ lies just below the 3d$_{3/2}$ of the MoO$_2$ feature. In addition, the binding energies at 54.2 and 55.0 eV in the Se 3d spectrum are characteristic of the Se^{2-} of MoSe$_2$ (figure 4(b)) [31]. Furthermore, the selenium-to-molybdenum stoichiometric ratio of Se and Mo of approximately 1:2 is obtained from the high-resolution XPS, suggesting that our CVD grown few-layer MoSe$_2$ is reasonably chemically stoichiometric.
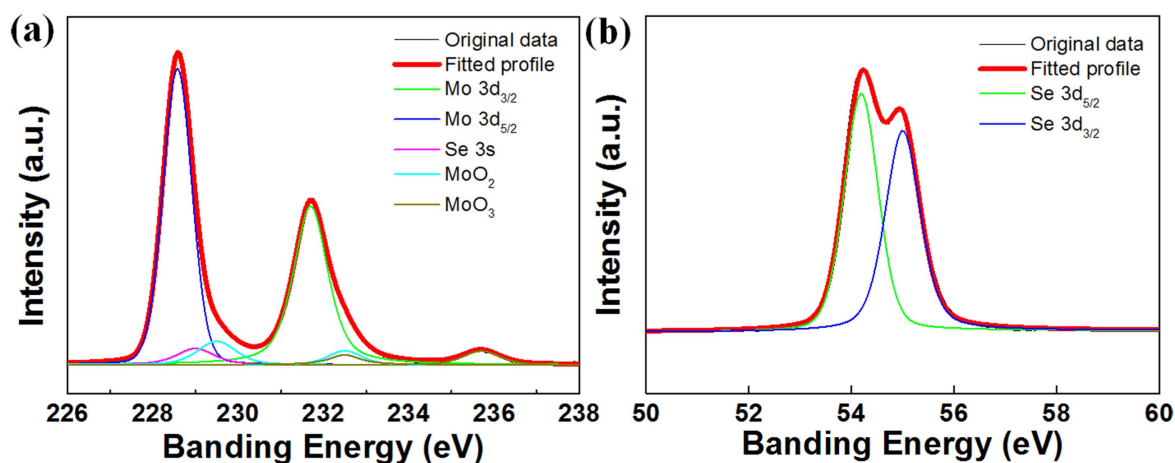
Figure 4. XPS spectra of MoSe$_2$ as-grown at 550 °C for 60 min. (a) XPS spectrum of Mo 3d and (b) XPS spectrum of Se 3d.

3.2. Growth mechanism of few-layer MoSe$_2$

The growth process of MoSe$_2$ film was explored by implementing the experiments as follows. (1) High-temperature pre-annealing was employed to improve the purity of Mo foils and enlarge the Mo grains, which facilitates controllably the reaction of Se with the Mo atoms on the substrate and makes the size of MoSe$_2$ atomic layers larger, similar to the pretreatment on the MoS$_2$ atomic layers [42]. (2) The influence of reaction time on the quality of few-layer MoSe$_2$ was investigated in detail. As mentioned above for the reaction at 550 °C (figure 2), it was observed that the thickness of the atomic layers was less than 5.0 nm for a reaction time within 30 min, uniform and thicker films with 6 nm in thickness were formed when prolonging the duration up to 60 min (figure S2(c)), while the thin MoSe$_2$ atomic layers when the duration reached 120 min (figures S2(a), (b) and (d)). The observation could be explained as follows: The deposition process was synergistically controlled by both surface and bulk diffusion at the reaction temperature. In addition, the process was also followed by the decomposition process of MoSe$_2$ thin films on Mo foils. With prolonging the reaction time up to 120 min, the selenium vapor concentration was reduced to a certain degree due to the loss of selenium powder in the source zone, which led to a reduction in thickness of MoSe$_2$ thin films because the decomposition rate is higher than the deposition rate. (3) The influence of reaction temperature on the quality of few-layer MoSe$_2$ was also probed. As the temperature was down to 350 °C, all of the produced thin films were discontinuous due to the inadequate reaction of the selenium source with the molybdenum substrate (figure S4). When the temperature was set to 450 °C, large-area and uniform films were only formed when the duration was below 10 min, and the thicker films were produced when prolonging the duration from 30 to 60 min (figure S5). When the temperature was set to over 650 °C for 30 min, large-area and uniform films were formed (figures S6(a) and (c)), however, discontinuous films were obtained after further prolonging the duration for more than 60 min owing to the adequate reaction of the selenium source with the molybdenum substrate (figures S6(b) and (d)). Overall, the dependence of growth of the as-synthesized

MoSe$_2$ thin films on the reaction temperature and time is summarized in figure S7.

Based on the experimental investigations, we propose a surface-diffusion-limited reaction mechanism to explain our experimental observations, similar to the proposed mechanism in our monolayer MoS$_2$ [42]. By contrast to the previous mechanism, the chemical reactivity of the precursor Se source is lower than that of the S source with Mo atomic surface [10, 26, 43]. Thus, it is necessary to extend the reaction time longer for large-scale synthesis of few-layer MoSe$_2$. Nevertheless, the long reaction time will inevitably lead to thicker films because the growth is not self-limiting, in contrast to the self-limited graphene grown on copper foil owing to the low solubility of carbon in copper [44]. In our experiments, the reaction temperature determines the solubility and the diffusion rate of Se atoms on the surface of Mo foils. The controllable preparation of MoSe$_2$ atomic layers is strongly dependent on the diffusion rates. According to the solid-state crystal growth theory, the few-layer MoSe$_2$ growth is controlled by both the surface diffusion rate and the bulk diffusion rate. The process can be understood as follows: in low reaction temperature, the Se atoms around the Mo foil surface will first precipitate where the surface diffusion rate of Se atoms on the Mo foil is higher than the bulk diffusion rate, and then the Se atoms reach a certain super-saturation and finally react with the top Mo atomic layers on the Mo foil; however, in high reaction temperature, the bulk diffusion rate of Se atoms on the Mo foil is higher than the surface diffusion rate, and thicker MoSe$_2$ thin films can be produced on Mo foils. From our experimental observations, MoSe$_2$ atomic layers are dominated by a surface diffusion mechanism when the reaction temperature is below 550 °C, while the atomic layers are controlled by a bulk diffusion mechanism when the reaction temperature is beyond 550 °C, for example, the thicker films can be produced at 650 °C. The systematic experiments indicated that the temperature of 550 °C is a controlled condition for preparing MoSe$_2$ atomic layers. It should be noted that for the growth performed at 550 °C, a slight variance in the thickness can be ascribed to the slightly balanced movement between the growth and decomposition
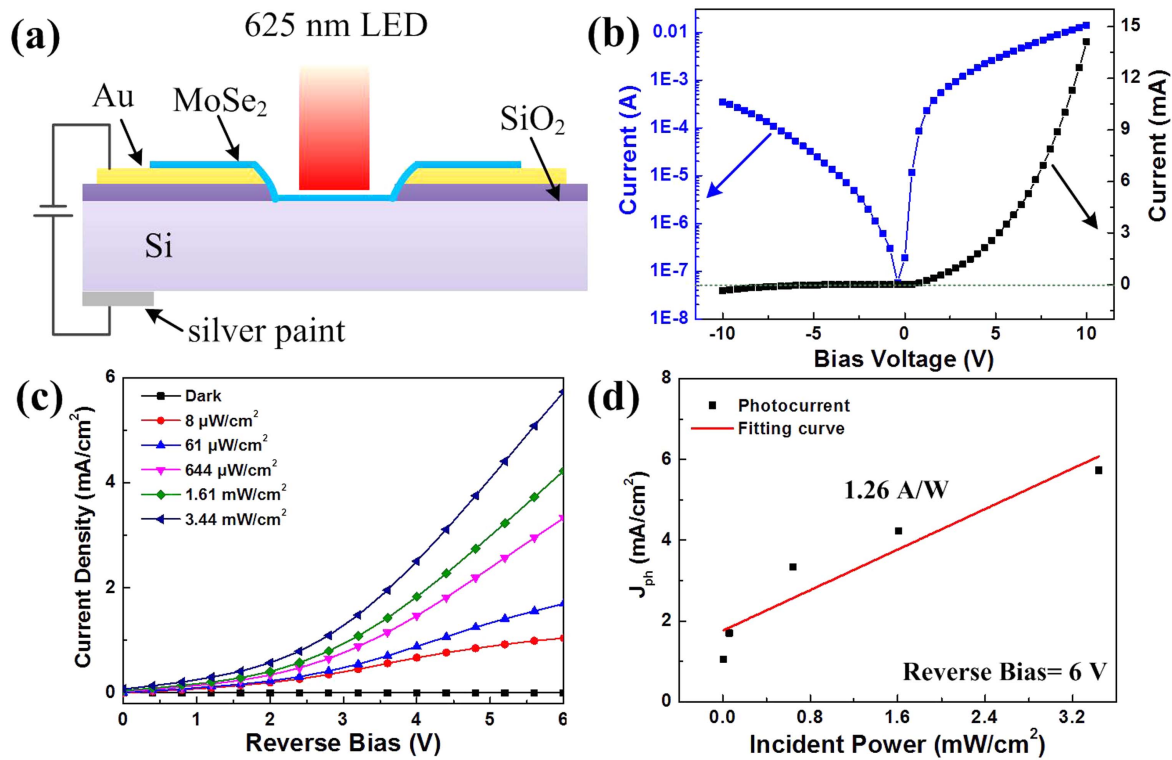
Figure 5. Photoelectric properties of few-layer $MoSe_2$. (a) Schematic view of a few-layer $MoSe_2$ photodetector under 625 nm LED illumination. (b) Current–voltage (I–V) characteristics and corresponding logarithmic curve of the device in the darkness, which shows good rectifying behavior. (c) Total current densities as a function of external reverse biases under varying incident light powers. (d) Photocurrent response of the $MoSe_2$–silicon photodetector as a function of the incident light power at a reverse bias of 6 V.

of the atomic layers. The thickness dependence of the $MoSe_2$ thin films on the reaction temperature is shown in figure S7. It is noteworthy that a complete understanding of the $MoSe_2$ growth process from theoretical viewpoints is still challenging. A thorough investigation of the atomistic mechanism for $MoSe_2$ atomic layer growth on Mo foils is a subject for future studies. However, regardless of the grain shapes and their reaction states, uniform $MoSe_2$ layers can be controllably prepared at 550 °C within 60 min.

3.3. Photodetection properties of few-layer $MoSe_2$–Si heterostructures

We selected few-layer $MoSe_2$ 6.0 nm in thickness grown at 550 °C for 60 min to fabricate the $MoSe_2$–Si photodetector. The vertical heterojunction device is composed of the few-layer $MoSe_2$ and p-type silicon (p-Si), as shown in figure 5(a). The device displays an obvious rectifying behavior in the darkness and the rectifying ratio measured at ±10 V is up to 41, as shown in figure 5(b). The rectification is due to the band bending occurring at the interface of $MoSe_2$ and p-Si, which induces the presence of a built-in potential that improves the excellent photoresponse performance of the device. To demonstrate the photodetection application of the device, we measured the photodetection properties under 625 nm LED illumination with various powers ranging from 8 μW mm^{-2} to 3.44 mW mm^{-2} (figure 5(c)). The good

electrical contact between $MoSe_2$ and the Au electrodes is confirmed by the obtained I–V plots. In sharp contrast to the electrical properties in the darkness, the current is significantly increased when the device was illuminated under LED light excitation and the values are strongly dependent on the power of the illuminating LED light source. It is observed that under the same bias, the larger the illuminated power is, the larger the photocurrent I_{ph} ($I_{ph} = I_{illuminated} - I_{dark}$) becomes due to the increased number of photon-generated carriers. Furthermore, photoresponsivity has been adopted to evaluate the photodetector performance. For the fabricated device in this work, the effective exposure area is designed to approximately 0.04 cm^2. Under the conditions of a LED power of 3.44 mW cm^{-2} and a bias voltage of 6 V, the photoresponsivity is calculated to be approximately 1.26 A W^{-1} (figure 5(d)), which is remarkably higher than that of the monolayer $MoSe_2$, MoS_2 and graphene phototransistors (13 mA W^{-1}) [29, 45, 46]. In contrast, the weak photoresponse of the device was measured under LED illuminations with 465 and 525 nm wavelength (figure S8). The results suggest that the strong photoresponse results from the enhanced band edge absorption of $MoSe_2$. The performance of the devices can be further improved by designing 2D materials heterostructures, optimizing the contact or using doping semiconducting quantum dots and silver or gold nanoparticles [47, 48].

4. Conclusion

In summary, we have demonstrated a large-area, uniform, high quality and easy transferable vapor transport deposition technique to synthesize highly crystalline $MoSe_2$ atomic layers on Mo foil in Se vapor at $550\,^{\circ}C$ within 60 min at atmospheric pressure with the assistance of Ar gas. A surface-diffusion-limited reaction mechanism was adopted to reasonably explain our experimental results. In contrast to the $MoSe_2$ atomic layers grown on insulating substrates, the obtained uniform layers can easily be transferred onto various substrates by removing the Mo foils using a diluted $FeCl_3$ solution. A p–n heterojunction device composed of the $MoSe_2$ layer and p-Si was fabricated to demonstrate its application in high-performance photodetectors. This study opens a novel route to synthesize TMD atomic layers on an industrial scale and facilitate their development in future sensing, memory and optoelectronic devices.

ORCID iDs

Guoan Tai https://orcid.org/0000-0002-9416-3753

References

[1] Mak K F, McGill K L, Park J and McEuen P L 2014 Valleytronics. The valley Hall effect in MoS_2 transistors *Science* **344** 1489–92

[2] Wu W Z *et al* 2014 Piezoelectricity of single atomic-layer MoS_2 for energy conversion and piezotronics *Nature* **514** 470–4

[3] Wang Q H, Kalantar-Zadeh K, Kis A, Coleman J N and Strano M S 2012 Electronics and opto-electronics of two-dimensional transition metal dichalcogenides *Nat. Nanotechnol.* **7** 699–712

[4] Rhyee J S *et al* 2016 High-mobility transistors based on large-area and highly crystalline CVD-grown $MoSe_2$ films on insulating substrates *Adv. Mater.* **28** 2316–21

[5] Zhang Y *et al* 2014 Direct observation of the transition from indirect to direct bandgap in atomically thin epitaxial $MoSe_2$ *Nat. Nanotechnol.* **9** 111–5

[6] Hao K *et al* 2017 Neutral and charged inter-valley biexcitons in monolayer $MoSe_2$ *Nat. Commun.* **8** 15552

[7] Cheng R, Jiang S, Chen Y, Liu Y, Weiss N, Cheng H C, Wu H, Huang Y and Duan X F 2014 Few-layer molybdenum disulfide transistors and circuits for high-speed flexible electronics *Nat. Commun.* **5** 5143

[8] Barja S *et al* 2016 Charge density wave order in 1D mirror twin boundaries of single-layer $MoSe_2$ *Nat. Phys.* **12** 751–6

[9] Kumar S and Schwingenschlögl U 2015 Thermoelectric response of bulk and monolayer $MoSe_2$ and WSe_2 *Chem. Mater.* **27** 1278–84

[10] Garciahernandez M and Coleman J 2016 Corrigendum: materials science of graphene: a flagship perspective *2D Mater.* **3** 010401

[11] Lu S C, Mohamed M and Zhu W 2016 Novel vertical hetero- and homo-junction tunnel field-effect transistors based on multi-layer 2D crystals *2D Mater.* **3** 011010

[12] Zhao H, Guo Q, Xia F and Wang H 2015 Two-dimensional materials for nanophotonics applic-ation *Nanophotonics* **4** 128–42

[13] Mak K F, Lee C, Hone J, Shan J and Heinz T F 2010 Atomically thin MoS_2: a new direct-gap semiconductor *Phys. Rev. Lett.* **105** 136805

[14] Butun S, Tongay S and Aydin K 2015 Enhanced light emission from large-area monolayer MoS_2 using plasmonic nanodisc arrays *Nano Lett.* **15** 2700–4

[15] Zhou X, Liu Y, Ju H, Pan B, Zhu J, Ding T, Wang C and Yang Q 2016 Design and epitaxial growth of $MoSe_2$-NiSe vertical heteronano-structures with electronic modulation for enhanced hydro-gen evolution reaction *Chem. Mater.* **28** 1838–46

[16] Kim S *et al* 2012 High-mobility and low-power thin-film transistors based on multilayer MoS_2 crystals *Nat. Commun.* **3** 1011

[17] Li D H, Cheng R, Zhou H L, Wang C, Yin A X, Chen Y, Weiss N O, Huang Y and Duan X F 2015 Electric-field-induced strong enhancement of electroluminescence in multilayer molybde-num disulfide *Nat. Commum.* **6** 7509

[18] Wang S X, Yu H H, Zhang H J, Wang A Z, Zhao M W, Chen Y X, Mei L M and Wang J Y 2014 Broadband few-layer MoS_2 saturable absorbers *Adv. Mater.* **26** 3538–44

[19] Cho K, Park W, Park J, Jeong H, Jang J, Kim T Y, Hong W K, Hong S and Lee T 2013 Electric stress-induced threshold voltage instability of multilayer MoS_2 field effect transistors *ACS Nano* **7** 7751–8

[20] Zhang E, Wang W, Zhang C, Jin Y, Zhu G, Sun Q, Zhang D W, Zhou P and Xiu F 2015 Tunable charge-trap memory based on few-layer MoS_2 *ACS Nano* **9** 612–9

[21] Yu F F, Liu Q W, Gan X, Hu M X, Zhang T Y, Li C, Kang F Y, Terrones M and Lv R T 2017 Ultrasensitive pressure detection of few-layer MoS_2 *Adv. Mater.* **29** 1603266

[22] Chen Y B *et al* 2017 Pressurizing field-effect transistors of few-layer MoS_2 in a diamond anvil cell *Nano Lett.* **17** 194–9

[23] Abderrahmane A, Ko P J, Thu T V, Ishizawa S, Takamura T and Sandhu A 2014 High photo-sensitivity few-layer $MoSe_2$ back-gated field-effect phototransistors *Nanotechnology* **25** 365202

[24] Tongay S, Zhou J, Ataca C, Lo K, Matthews T S, Li J, Grossman J C and Wu J 2012 Thermally driven crossover from indirect toward direct bandgap in 2D semiconductors: $MoSe_2$ versus MoS_2 *Nano Lett.* **12** 5576–80

[25] Hu F, Luan Y, Scott M E, Yan J, Mandrus D G, Xu X and Fei Z 2017 Imaging exciton-polariton transport in $MoSe_2$ waveguides *Nat. Photon.* **11** 356–60

[26] Lu X *et al* 2014 Large-area synthesis of mono-layer and few-layer $MoSe_2$ films on SiO_2 sub-strates *Nano Lett.* **14** 2419–25

[27] Chen J *et al* 2017 Chemical vapor deposition of large-size monolayer $MoSe_2$ crystals on molten glass *J. Am. Chem. Soc.* **139** 1073–6

[28] Kong D S, Wang H T, Cha J J, Pasta M, Koski K J, Yao J and Cui Y 2013 Synthesis of MoS_2 and $MoSe_2$ films with vertically aligned layers *Nano Lett.* **13** 1341–7

[29] Xia J, Huang X, Liu L Z, Wang M, Wang L, Huang B, Zhu D D, Li J J, Gu C Z and Meng X M 2014 CVD synthesis of large-area, highly crystalline MoSe$_2$ atomic layers on diverse substrates and application to photodetectors *Nanoscale* **6** 8949–55

[30] Poh S M *et al* 2017 Large area synthesis of 1D-MoSe$_2$ using molecular beam epitaxy *Adv. Mater.* **29** 1605641

[31] Wang X *et al* 2014 Chemical vapor deposition growth of crystalline monolayer MoSe$_2$ *ACS Nano* **8** 5125–31

[32] Bradley A J *et al* 2015 Probing the role of interlayer coupling and coulomb interactions on electronic structure in few-layer MoSe$_2$ nanostructures *Nano Lett.* **15** 2594–9

[33] Gong Y J *et al* 2015 Two-step growth of two-dimensional WSe$_2$/MoSe$_2$ heterostructures *Nano Lett.* **15** 6135–41

[34] Soubelet P, Bruchhausen A E, Fainstein A, Nogajewski K and Faugeras C 2016 Resonance effects in the Raman scattering of monolayer and few-layer MoSe$_2$ *Phys. Rev.* B **93** 155407

[35] Lee C, Yan H, Brus L E, Heinz T F, Hone J and Ryu S 2010 Anomalous lattice vibrations of single- and few-layer MoS$_2$ *ACS Nano* **4** 2695–700

[36] Lei S, Ge L, Liu Z, Najmaei S, Shi G, You G, Lou J, Vajtai R and Ajayan P M 2013 Synthesis and photoresponse of large GaSe atomic layers *Nano Lett.* **13** 2777–81

[37] Lee Y H *et al* 2012 Synthesis of large-area MoS$_2$ atomic layers with chemical vapor deposition *Adv. Mater.* **24** 2320–5

[38] Ferrari A C and Basko D M 2013 Raman spectroscopy as a versatile tool for studying the properties of graphene *Nat. Nanotechnol.* **8** 235–46

[39] Wang H, Yu L, Lee Y H, Shi Y, Hsu A, Chin M L, Li L J, Dubey M, Kong J and Palacios T 2012 Integrated circuits based on bilayer MoS$_2$ transistors *Nano Lett.* **12** 4674–80

[40] Sun D, Feng S, Terrones M and Schaak R E 2015 Formation and interlayer decoupling of colloidal MoSe$_2$ nanoflowers *Chem. Mater.* **27** 3167–75

[41] Gong Y J *et al* 2016 Synthesis of millimeter-scale transition metal dichalcogenides single crystals *Adv. Funct. Mater.* **26** 2009–15

[42] Tai G A, Zeng T, Yu J, Zhou J X, You Y C, Wang X F, Wu H R, Sun X, Hu T S and Guo W L 2016 Fast and large-area growth of uniform MoS$_2$ monolayers on molybdenum foils *Nanoscale* **8** 2234–41

[43] Tsirlina T, Feldman Y, Homyonfer M, Sloan J, Hutchison J L and Tenne R 1998 Synthesis and characterization of inorganic fullerene-like WSe$_2$ material *Fullerene Sci. Technol.* **6** 157–65

[44] Li X S *et al* 2009 Large-area synthesis of high-quality and uniform graphene films on copper foils *Science* **324** 1312–4

[45] Mueller T, Xia F and Avouris P 2010 Graphene photodetectors for high-speed optical communications *Nat. Photonics* **4** 297–301

[46] Yin Z, Li H, Li H, Jiang L, Shi Y, Sun Y, Lu G, Zhang Q, Chen X and Zhang H 2012 Single-layer MoS$_2$ phototransistors *ACS Nano* **6** 74–80

[47] Liu Z K, Li J H, Sun Z H, Tai G, Lau S P and Yan F 2012 The application of highly doped single-layer graphene as the top electrodes of semitransparent organic solar cells *ACS Nano* **6** 810–8

[48] Sun Z H, Liu Z K, Li J H, Tai G, Lau S P and Yan F 2012 Infrared photodetectors based on CVD-grown graphene and PbS quantum dots with ultrahigh responsivity *Adv. Mater.* **24** 5878–83